Title

A Metabolomics Study of Hypoxia Ischemia during Mouse Brain Development Using Hyperpolarized 13C

Journal

Developmental Neuroscience, 42(1)

ISSN

0378-5866

Authors

Mikrogeorgiou, Alkisti
Chen, Yiran
Lee, Byong Sop
et al.

Publication Date

2020

DOI

10.1159/000506982

Peer reviewed

HHS Public Access

Author manuscript

Dev Neurosci. Author manuscript; available in PMC 2021 June 22.

Published in final edited form as:

Dev Neurosci. 2020 ; 42(1): 49–58. doi:10.1159/000506982.

A metabolomics study of hypoxia ischemia during mouse brain development using hyperpolarized ^{13}C

Alkisti Mikrogeorgiou[1], **Yiran Chen**[2,3], **Byong Sop Lee**[4], **Robert Bok**[2], **R Ann Sheldon**[1], **A James Barkovich**[2,5], **Duan Xu**[2,3], **Donna M Ferriero**[1]

[1]Department of Neurology, University of California, San Francisco, USA

[2]Department of Radiology and Biomedical Imaging, University of California San Francisco, USA

[3]Joint UCSF/UC Berkeley Graduate Group in Bioengineering, USA

[4]Department of Pediatrics, Asan Medical Center, University of Ulsan College of Medicine, Seoul, Korea

[5]Department of Pediatrics, University of California, San Francisco, USA

Abstract

Background: Hyperpolarized ^{13}C spectroscopic magnetic resonance imaging is an advanced imaging tool that may provide important real time information about brain metabolism.

Methods: Mice underwent unilateral hypoxia-ischemia (HI) on postnatal day 10 (P10). Injured and sham mice were scanned at P10, postnatal day 17 (P17), and postnatal day 31 (P31). We used hyperpolarized ^{13}C spectroscopic magnetic resonance imaging (^{13}C MRS) to investigate the metabolic exchange of pyruvate to lactate in real-time during brain development following HI. ^{13}C-1 labeled pyruvate was hyperpolarized and injected into the tail vein through a tail-vein catheter. Chemical-shift imaging (CSI) was performed to acquire spectral-spatial information of the metabolites in the brain. A voxel placed on each of the injured and contralateral hemispheres was chosen for comparison. The difference in pyruvate delivery and lactate to pyruvate ratio was calculated for each of the voxels at each time point. The normalized lactate level of the injured hemisphere was also calculated for each mouse at each of the scanning time points.

Results: There was a significant reduction in pyruvate delivery and a higher lactate to pyruvate ratio in the ipsilateral (HI) hemisphere at P10. The differences decreased at P17 and disappeared at P31. The normalized lactate level in the injured hemisphere increased from P10 to P31 in both sham and HI mice without brain injury.

Corresponding author: Duan Xu, PhD, Imaging Research for Neurodevelopment Laboratory, University of California San Francisco, 1700 4th St, BH102, UCSF Box 2512, San Francisco, CA 94158, Phone: +1 415-476-5978, Fax: +1 415-514-4451, duan.xu@ucsf.edu.

Author Contributions

Dr. Alkisti Mikrogeorgiou, Dr. Yiran Chen and Dr. Byong Sop Lee contributed equally in the writing of this manuscript and the realization of this study.

Statement of Ethics

All animal experiments were approved by the University of California San Francisco (UCSF) institutional animal care and use committee.

Disclosure Statement

The authors declare they have no conflicts of interest.

Conclusion: We describe a method for detecting and monitoring evolution of HI injury during brain maturation which could prove to be an excellent biomarker of injury.

Keywords

developing brain; hyperpolarized ^{13}C; metabolism; MRS; neonatal brain injury; pyruvate; lactate

Introduction

Hypoxia-ischemia (HI) is an important cause of neonatal mortality and morbidity. Mechanisms of HI-induced brain damage have been studied on both cellular and molecular levels [1–4]. The emergence of magnetic resonance imaging (MRI) provides a non-invasive way to examine brain structures *in vivo,* allowing longitudinal studies to be performed to assess long-term responses. The majority of MRI studies in HI animals are based on structural images such as T1-weighted, T2-weighted and diffusion tensor imagining [5–7]. A few MR studies have focused on the metabolic properties of HI using ^{1}H or ^{31}P spectroscopy [8–10]. ^{13}C spectroscopy provides yet another perspective, allowing investigation of metabolic exchange and labeled neurotransmitters such as glutamate, GABA and aspartate in the developing murine brain [11–13].

Naturally, the sensitivity of the ^{13}C nucleus is low because its natural abundance is only about 1% in living organisms and is therefore hard to detect within a limited scan time. Thus, most of the ^{13}C MRS studies require a long scan time, which can only be achieved in cell culture and extracted tissues [14–17], restricting the feasibility of longitudinal experiments to study long-term developmental responses after the injury to the immature brain. Some of the *in vivo* studies require constant infusion of metabolites for minutes or hours [18,19], which is practically impossible to achieve in neonatal mice small blood volumes. Moreover, the long scan time hinders the capability of measuring dynamic changes of metabolites.

In 2003 Golman et al [20] introduced a new method to dynamically quantify metabolism using hyperpolarized ^{13}C, which enabled an entirely different avenue to study metabolism *in vivo* in real-time. Dynamic nuclear polarization (DNP) has been proven to increase ^{13}C NMR signal more than 10,000-fold, allowing investigation of ^{13}C metabolic exchanges in vivo [21]. DNP is based on polarizing the nuclear spins of a molecule in the solid state. It requires unpaired electrons, usually provided in the form of organic free radicals. Microwave irradiation at low temperature is then used to transfer the high electron polarization spins to the nuclei. Once a hyperpolarized substrate is injected into a living mammal, real-time ^{13}C metabolic imaging is performed to study metabolism by following the substrate as it participates in a biochemical process. However, the hyperpolarization of the nuclear spin returns to thermal equilibrium after a very short time at room temperature. Therefore, a metabolite must be carefully chosen in order to visualize the metabolic pathway within this time period. Hyperpolarized ^{13}C-1 labeled pyruvate has been used to track metabolism in vivo, in rodents [22], non-human primates [23] and humans [24,25], due to its rapid delivery and uptake by the cells in various organs, and its quick conversion into lactate, alanine and/or carbon dioxide through various metabolic pathways.

Cerebral energy failure has been broadly recognized as the main initiating event resulting in cell death and the evolution of HI injury. Therefore, in this study, we applied DNP using ^{13}C-1 labeled pyruvate to investigate the changes in the conversion of pyruvate to lactate following HI in newborn mice during brain maturation in vivo, in order to examine ongoing metabolic exchanges during early brain development.

Methods

Hypoxia-ischemia

P10 male and female CD1 mice were subjected to HI as previously described according to the Vannucci model [26]. All procedures were approved by the Institutional Animal Care and Use Committee at the University of California San Francisco, in accordance with National Institutes of Health guidelines for the Care and Use of Laboratory Animals. Ligation of the left common carotid artery was performed as follows: Animals were anesthetized with 3.5% isoflurane. A midline neck incision was done in order to separate and permanently ligate the left common carotid artery via electrical coagulation. After the procedure, pups were allowed 1 h recovery with the dam. Global hypoxia was induced by placing the pups in chambers submerged in a water bath at 37°C into which a hypoxic atmosphere of 10% O2 / 90% N2 was introduced via inlet and outlet tubing controlled by a flow meter. After 60 minutes, pups were returned to the dam.

MRI

A total of 10 mice were subjected to HI. They were scanned at P10 (2–5 hours post HI), P17, and P30-P32. Some dates were slightly shifted or missing due to scanner availability, technical issues or animal expiration (n = 2). 3 mice were added at the second timepoint of the study. A total of 5 sham mice were also scanned at the same time points. These time points were chosen to span murine brain maturation with P10 being equivalent to human term infants, P17 being representative of early childhood, and P31 being representative of adolescence [27–29].

Mice were anesthetized with 1.5% isoflurane and 1 L/min oxygen during scans. A catheter was inserted into the tail vein for intravenous injection of hyperpolarized pyruvate. During the imaging experiment, 0.3mL of mixed saline and heparin was injected into the catheter every 15 minutes to prevent blood clots. All experiments were conducted on a vertical 14.1T (Agilent) 600WB NMR spectrometer with 55mm 1000mT/m gradients. A 38mm diameter ^{1}H and ^{13}C dual-tuned coil was used, for main field shimming and T2-weighted anatomical imaging (^{1}H frequency), and for hyperpolarized ^{13}C spectroscopic imaging (^{13}C frequency).

48μL of C-1 labeled ^{13}C pyruvic acid was polarized in an Oxford Hypersense™ DNP instrument at 3.5T under 1.5K for an hour. Before injecting the pyruvate sample into the mouse, the hyperpolarized ^{13}C-1 pyruvate was mixed with 4.5mL of NaOH buffer, which resulted a 160mM pyruvate solution with pH~7.5. The dissolution mixture was then injected into the tail vein through a catheter over a span of 12 seconds. The total volume injected was 300 μL with 150 μL into the mouse and 150 μL left in the catheter.

Data acquisition

^{13}C spectroscopic imaging—Data were acquired on a 24mm×24mm×5mm slice centered on the brain, with 2D chemical-shift imaging. Center-out k-space trajectory was used with 8 × 8 phase encoding. 128 spectral points were acquired with 2500 Hz bandwidth. From our previous hyperpolarized ^{13}C-1 pyruvate study on young mouse brains with the same experimental procedure, pyruvate signal reaches its peak at around 12 to 16 seconds after the beginning of the injection [30]. In this study, acquisition was initiated 10 seconds after the pyruvate injection, so the first time point coincides with when pyruvate is at its highest level. The acquisition was repeated every 5s (4s acquisition time with 1s delay between each repetition) for a total of 75s (or 15 repetitions) with constant flip angle of 10° (Figure 2).

T2-weighted anatomical imaging—A 2D fast spin echo (FSE) sequence was applied for anatomical imaging with TR/TE=1.3 s/12 ms, and 8 echo train length with 12 ms echo spacing. The field of view was 30 mm × 30 mm with 256 frequency and phase encodes, resulting in a 0.12 mm × 0.12 mm in-plane resolution. The slice thickness was 1 mm, and 10 slices were acquired without gap, covering most of the brain. The total scan time was 11 minutes.

Evaluation of brain damage—We scored the extent of damage in each animal at P17 based on the T2-weighted images. Some mice were missing scans at either P10 or P31 due to technical problems or death, but all mice were scanned at P17. The injury at P10, which was depicted as hypointensity, extended almost to the entire ipsilateral hemisphere and had very little contrast or localization (Figure 1); therefore, it was difficult to score. The injury pattern at P31 was similar to the injury at P17.

Our scores were based on the 3 major injury areas: cortex, hippocampus, and deep gray nuclei. Each area was scored rostral to caudal by progressively increasing numerical scores, which denoted either lack of injury, mild, moderate or severe damage. More specifically, each area was scored from 0–3 based on the following: 0 for no injury observed, 1 for mild focal hyperintensity, 2 for moderate larger hyperintensity that expanded to adjacent areas, and 3 for cystic infarction. The total score was the sum of the 3 areas and ranged from 0 to 9.

Data processing and analysis

Voxel shift was performed on the 2D grid to locate one voxel on the left hemisphere and one voxel on the right hemisphere (Figure 1). The area under the peak of pyruvate and lactate was recorded for each of the 15 time points for the construction of the dynamic curves (Figure 2).

Pyruvate delivery—The area under the pyruvate curve and the lactate curve were taken from a voxel on each of the hemispheres. The pyruvate signal intensity depended on the polarization level, which varied between experiments. In order to examine the effect of HI on pyruvate delivery into the brain, we compared the absolute pyruvate level between the two voxels chosen on each of the hemispheres. The pyruvate signal difference between two

hemispheres was calculated as $Diff_{pyr} = \frac{pyr_R - pyr_L}{pyr_R + pyr_L}$, where Pyr_R is the area under the pyruvate curve for the right hemisphere and Pyr_L for the left hemisphere. We conducted a student t-test for comparing $Diff_{pyr}$ between HI and Sham groups at each age.

Lactate to pyruvate ratio—The lactate signal intensity is affected by the amount of pyruvate delivery, as pyruvate and lactate levels quickly equilibrate in the brain. Small increases of lactate in the brain may represent lactate-pyruvate equilibration rather than indicating excessive production of lactate [31]. Therefore, in order to observe changes in the pyruvate conversion to lactate due to HI, we compare the lactate to pyruvate ratio between the two voxels chosen on each of the hemispheres. The difference in lactate to pyruvate ratio were calculated as $Diff_{ratio} = \frac{Ratio_R - Ratio_L}{Ratio_R + Ratio_L}$, where $Ratio_R$ is the ratio of the area under the lactate curve to the area under the pyruvate curve for the right hemisphere and $Ratio_L$ is calculated the same for the left hemisphere. We conducted student t-test for the comparison of $Diff_{ratio}$ between HI and Sham groups at each age.

Normalized lactate level in the brain—In our previous study on utilizing hyperpolarized ^{13}C-1 pyruvate during normal brain maturation, we have found that the conversion from pyruvate to lactate slows down as the brain ages beyond P18 [30]. In this study, we examined this metabolic exchange at an additional time point, at P10. This allowed us to examine the metabolic conversion changes from the neonatal period (P10) to early childhood (P17), and from early childhood to adolescence (P31). We further plotted the normalized lactate level in the injured hemisphere, against age for each HI and sham mouse, in order to examine the longitudinal change of the average lactate signal. For this purpose, we used the same analysis method described in our previous study [30], by selecting the voxel centered on the injured side of the brain and calculating the normalized lactate level, which is the average lactate signal in the left voxel, divided by the total ^{13}C signal (Figure 5).

Results

Figure 1 shows the T2-weighted image and spectra after voxel shift for a representative HI subject at each age. A slight hypointensity can be observed in the hemisphere ipsilateral to the carotid ligation (HI) and a significant reduction of pyruvate delivery in the spectra in the injured hemisphere a few hours after HI at P10. At P17 and P31, there are well-defined areas of hyperintensity in the injured hemisphere. At this age, the pyruvate delivery to the injured side appears to have slightly recovered so that the difference between the two hemispheres is not statistically significant (pyn_L versus pyr_R, p=0.165 at P17) and that difference continues to diminish at P31 (pyn_L versus pyr_R p= 0.4256).

HI brain damage

The HI injury scores of all the mice are shown in Table 1. The animals in this study were either normal (score = 0, n = 3), mildly injured (score = 1 to 2, n = 2), or severely injured (score = 6 to 9, n = 5). We combined the HI subjects with no injury (n = 3) with the sham

operated subjects (n = 5) to depict the longitudinal change of normalized lactate level in the brain (Figure 5).

Pyruvate delivery

Figure 3(a) shows the plot of $Dif\ f_{pyr}$ against age for each animal. All HI mice have positive values of $Dif\ f_{pyr}$ at P10, which can be interpreted as less pyruvate delivered to the left hemisphere (ipsilateral) than the right hemisphere (contralateral). The difference between the two hemispheres decreases at P17 as $Dif\ f_{pyr}$ values approach zero. There is no difference between the two hemispheres at P31 since $Dif\ f_{Pyr}$ values are nearly nullified. However, no differences are observed in the sham group, as all subjects have all $Dif\ f_{pyr}$ values around zero at each age. Figure 3(b) shows the Student t-test results between HI and sham groups at each age, with $p<0.01$ at P10, $p<0.05$ at P17 and no statistical significance at P31.

Lactate to pyruvate ratio

Although the HI hemisphere has a lower pyruvate level, its lactate to pyruvate ratio is higher at P10 (Figure 4a) for most of the mice, as indicated by negative $Dif\ f_{ratio}$ values. Again, this difference between two hemispheres diminishes as the brain matures to P17 and P31. There is no difference shown in the sham group in terms of lactate to pyruvate ratio. To further confirm our observation, Figure 4(b) shows the Student t-test results with $p<0.01$ at P10 and no statistical significance at P17 and P31 between the HI and sham groups.

Normalized lactate level in the injured hemisphere

Figure 5 shows the plot of individual normalized lactate levels in the left hemisphere (Normalized Lao.) against age. A general pattern for sham subjects can be discerned as the normalized lactate increases from P10 to P31 (Figure 5c). However, this pattern is not consistent in the HI group. Figure 5b shows the same data as Figure 5(a) but the HI animals are colored into 2 subgroups based on their HI injury scores. Animals with no injury (score = 0) have the same normalized lactate level change across age as the sham subjects, while most of the severely injured animals (score = 6 to 9) do not preserve the same trend.

Discussion

To our knowledge, this is the first study to characterize the metabolic profile of the murine brain after HI injury and to analyze its evolution over time, using hyperpolarized ^{13}C MRS. From the injury scores in Table 1, and the T2-weighted images in Figure 1, we could only observe non-localized hypointensity throughout the entire ipsilateral hemisphere 2 to 5 hours after HI. Previous MRI studies, on HI rats and mice, have shown evidence of decreased apparent diffusion coefficient (ADC) values in the regions corresponding to the lesion 3–24 h post-HI [6]. Below-normal ADC values appear as hypointensity on T2-weighted images and can be interpreted as edema and inflammation [32]. It has been documented that the inflammation by neutrophil accumulation in brain blood vessels peaks at 4 to 8 hours after reperfusion in neonatal HI rats [33], and that it can lead to further brain injury and cell death. At P17 and P31, the injury is more apparent and can be seen as extended hyperintensity in parts, or all of the cortex, hippocampus, and deep gray nuclear regions.

From both visual observation (Figure 1) and statistical analyses (Figure 3(b)) it is apparent that there is prominent reduction of pyruvate delivery to the ipsilateral hemisphere at 2–5 h after the insult. The lack of blood flow from vascular damage, right after HI, hinders the pyruvate delivery to the ipsilateral hemisphere. During the course of HI, oxygen supply is reduced due to the diminished blood flow to the ipsilateral hemisphere. Thus, aerobic glycolysis must be compensated with anaerobic energy production, through the reduction of pyruvate into lactate. This leads to an excess of protons (NADH molecules) and thus to the fall in tissue pH [34,35]. According to our results, the lactate to pyruvate ratio is higher in the ipsilateral voxel, suggesting a shift of the pyruvate - lactate equilibrium towards lactate formation, which is in agreement with the cerebral lactic acidosis that has been reported to occur after neonatal HI [36].

The difference between the ipsilateral and contralateral hemispheres in pyruvate delivery and lactate to pyruvate ratio decreases during brain maturation following HI, with a less significant difference at P17. The brain usually returns to normal aerobic metabolism about 1 h after HI [37,38]. The high lactate to pyruvate ratio at P10 likely reflects the aftermath of anaerobic glycolysis during the hypoxic episode. Thus, at that point (~2 to 5 hours after HI), the brain could still be partially dependent upon anaerobic metabolism, especially in the context of a severe injury, where the tricarboxylic acid cycle is compromised due to mitochondrial damage [4,39]. At P17, there is tissue loss seen as cystic infarction, as well as growth of normal tissue with aerobic and minimal anaerobic glycolysis, and therefore, less difference in lactate to pyruvate ratio between the hemispheres.

Even though the T2-weighted images show ipsilateral cystic infarction at P31, there is no statistical significance in $Dif\,f_{pyr}$ and $Dif\,f_{ratio}$ between the HI and sham groups. This may suggest that the non-injured regions on the ipsilateral hemisphere compensate for the injured regions in blood flow and energy consumption, and result in negating any differences in pyruvate delivery and lactate to pyruvate ratio between the two hemispheres.

One limitation of this study is that the voxel size was $3 \times 3 \times 5$ mm^3, so that we were only able to place one voxel on each hemisphere, which means that the ipsilateral measurement also included normal (non-injured) brain tissue. Low spatial resolution has been a technical challenge in hyperpolarized ^{13}C studies, especially in dynamic measurements with short acquisition time (TR was 4 s in this study). Moreover, the T1 of the hyperpolarized substrate is shorter at the higher field strength of our 14T animal scanner as compared to lower fields such as 1.5T or 3T. Therefore, there is a tradeoff between spatial resolution and temporal resolution. With future advancements in acquisition techniques, higher spatial resolution may be achievable. With smaller voxels, we will be able to distinguish localized injury from its surrounding non-injured area and make a more comprehensive interpretation of ^{13}C substrate uptake and conversion.

In our previous study of utilizing hyperpolarized ^{13}C during normal brain maturation, we began measurements at P18 [30]. In this study, the addition of a time point at P10 allowed us to investigate how the brain matures metabolically from the neonatal period to childhood and from childhood to adolescence [27–29] as well as determine how it responds immediately to injury. Although the HI group does not show the same general trend of

lactate production as the sham group in Figure 5(a) and 5(c), when the HI mice are divided into two distinct subgroups based on the injury score as shown in Figure 5(b), it is clear that the HI subgroup with no injury (score = 0) exhibit the same trend as the sham group. This is consistent with our previous findings of a decreasing conversion rate of pyruvate to lactate, starting at P18 [30]. A previous *in situ* study showed that the expression of the monocarboxylate transporter (MCT1 and MCT2) mRNAs, upon which lactate and pyruvate delivery and utilization in the brain depends, increases from P0, peaks at P15, decreases at P30 and stabilizes after [40]. Both these findings and our study agree on the extent of pyruvate and lactate delivery in normal brain maturation, which increases from the neonatal period to childhood and drops after weaning. The HI subgroup with high injury scores (6 to 9) do not show a general increase of lactate production from P10 to P17, which may due to the lack of metabolically active tissue at the injury site.

Conclusion

Our study employs a novel method for evaluating HI, by focusing on the exchange of pyruvate to lactate *in vivo* in real-time. Using hyperpolarized ^{13}C-1 pyruvate MRS, we have demonstrated metabolic changes during brain maturation and in the setting of HI brain injury. The differences observed suggest that this technique may be a useful way to detect metabolic biomarkers, since early detection of injury with conventional MRI is not always possible or predictive of the extent of brain damage. Continued investigations will be necessary to elucidate the complex interplay in lactate production and uptake, between the different brain regions and to correlate these metabolic perturbations with long-term outcomes.

Acknowledgments

We thank Dr. Susan Vannucci for the helpful comments and linguistic editing.

Funding sources

The authors are grateful to the NIH/NINDS (grant #R35NS097299 to Donna M. Ferriero) for the financial support.

References

1. McLean C, Ferriero D. Mechanisms of hypoxic-ischemic injury in the term infant. Semin Perinatol. 2004 DOI: 10.1053/j.semperi.2004.10.005
2. Mishra OP, Delivoria-Papadopoulos M. Cellular mechanisms of hypoxic injury in the developing brain. Brain Res Bull. 1999 DOI: 10.1016/S0361-9230(98)00170-1
3. Vannucci SJ, Hagberg H. Hypoxia-ischemia in the immature brain. J Exp Biol. 2004 DOI: 10.1242/jeb.01064
4. Northington FJ, Chavez-Valdez R, Martin LJ. Neuronal cell death in neonatal hypoxia-ischemia. Ann Neurol. 2011 DOI: 10.1002/ana.22419
5. Tuor UI, Kozlowski P, Del Bigio MR, Ramjiawan B, Su S, Malisza K, et al. Diffusion- and T2-weighted increases in magnetic resonance images of immature brain during hypoxia-ischemia: Transient reversal posthypoxia. Exp Neurol. 1998 DOI: 10.1006/exnr.1997.6766
6. Ådén U, Dahlberg V, Fredholm BB, Lai LJ, Chen Z, Bjelke B. MRI evaluation and functional assessment of brain injury after hypoxic ischemia in neonatal mice. Stroke. 2002 DOI: 10.1161/01.STR.0000014608.78503.DB

7. Burnsed JC, Chavez-Valdez R, Hossain MS, Kesavan K, Martin LJ, Zhang J, et al. Hypoxia-ischemia and therapeutic hypothermia in the neonatal mouse brain - A longitudinal study. PLoS One. 2015 DOI: 10.1371/journal.pone.0118889
8. Kauppinen RA, Williams SR. Nuclear magnetic resonance spectroscopy studies of the brain. Prog Neurobiol. 1994 DOI: 10.1016/0301-0082(94)90058-2
9. Pfeuffer J, Tkáč I, Provencher SW, Gruetter R. Toward an in Vivo Neurochemical Profile: Quantification of 18 Metabolites in Short-Echo-Time^{1}H NMR Spectra of the Rat Brain. J Magn Reson. 1999 DOI: 10.1006/jmre.1999.1895
10. Kloiber O, Miyazawa T, Hoehn-Berlage M, Hossmann K-A. Simultaneous ^{31}P NMR spectroscopy and laser doppler flowmetry of rat brain during global ischemia and reperfusion. NMR Biomed. 1993 DOI: 10.1002/nbm.1940060207
11. Morken TS, Brekke E, Håberg A, Widerøe M, Brubakk AM, Sonnewald U. Neuron-astrocyte interactions, pyruvate carboxylation and the pentose phosphate pathway in the neonatal rat brain. Neurochem Res. 2014 DOI: 10.1007/s11064-013-1014-3
12. Chowdhury GMI, Patel AB, Mason GF, Rothman DL, Behar KL. Glutamatergic and GABAergic neurotransmitter cycling and energy metabolism in rat cerebral cortex during postnatal development. J Cereb Blood Flow Metab. 2007 DOI: 10.1038/sj.jcbfm.9600490
13. Novotny EJ, Ariyan C, Mason GF, O'Reilly J, Haddad GG, Behar KL. Differential increase in cerebral cortical glucose oxidative metabolism during rat postnatal development is greater in vivo than in vitro. Brain Res. 2001 DOI: 10.1016/S0006-8993(00)03051-1
14. Hassel B, Bråthe A. Cerebral metabolism of lactate in vivo: Evidence for neuronal pyruvate carboxylation. J Cereb Blood Flow Metab. 2000 DOI: 10.1097/00004647-200002000-00014
15. Waagepetersen HS, Bakken IJ, Larsson OM, Sonnewald U, Schousboe A. Comparison of lactate and glucose metabolism in cultured neocortical neurons and astrocytes using 13C-NMR spectroscopy. Developmental Neuroscience. 1998 DOI: 10.1159/000017326
16. Alves PM, McKenna MC, Sonnewald U. Lactate metabolism in mouse brain astrocytes studied by [13C]NMR spectroscopy. Neuroreport. 1995 DOI: 10.1097/00001756-199511000-00024
17. Bouzier-Sore AK, Voisin P, Canioni P, Magistretti PJ, Pellerin L. Lactate Is a Preferential Oxidative Energy Substrate over Glucose for Neurons in Culture. J Cereb Blood Flow Metab. 2003 DOI:10.1097/01.WCB.0000091761.61714.25
18. Cerdan S, Kunnecke B, Seelig J. Cerebral metabolism of [1,2–13C2]acetate as detected by in vivo and in vitro 13C NMR. J Biol Chem. 1990 DOI: 10.1038/175779a0
19. Sibson NR, Dhankhar a, Mason GF, Behar KL, Rothman DL, Shulman RG. In vivo 13C NMR measurements of cerebral glutamine synthesis as evidence for glutamate-glutamine cycling. Proc Natl Acad Sci U S A. 1997 DOI: 10.1073/pnas.94.6.2699
20. Golman K, Ardenkjaer-Larsen JH, Petersson JS, Mansson S, Leunbach I. Molecular imaging with endogenous substances. Proc Natl Acad Sci. 2003 DOI: 10.1073/pnas.1733836100
21. Ardenkjaer-Larsen JH, Fridlund B, Gram A, Hansson G, Hansson L, Lerche MH, et al. Increase in signal-to-noise ratio of > 10,000 times in liquid-state NMR. Proc Natl Acad Sci. 2003 DOI:10.1073/pnas.1733835100
22. Golman K, in 't Zandt R, Thaning M. Real-time metabolic imaging. Proc Natl Acad Sci. 2006 DOI: 10.1073/pnas.0601319103
23. Park I, Bok R, Ozawa T, Phillips JJ, James CD, Vigneron DB, et al. Detection of early response to temozolomide treatment in brain tumors using hyperpolarized 13C MR metabolic imaging. J Magn Reson Imaging. 2011 DOI: 10.1002/jmri.22563
24. Park I, Larson PEZ, Gordon JW, Carvajal L, Chen HY, Bok R, et al. Development of methods and feasibility of using hyperpolarized carbon-13 imaging data for evaluating brain metabolism in patient studies. Magn Reson Med. 2018 DOI: 10.1002/mrm.27077
25. Nelson SJ, Kurhanewicz J, Vigneron DB, Larson PEZ, Harzstark AL, Ferrone M, et al. Metabolic imaging of patients with prostate cancer using hyperpolarized [1–13C]pyruvate. Sci Transl Med. 2013 DOI: 10.1126/scitranslmed.3006070
26. Rice JE, Vannucci RC, Brierley JB. The influence of immaturity on hypoxic-ischemic brain damage in the rat. Ann Neurol. 1981 DOI: 10.1002/ana.410090206

27. Semple BD, Blomgren K, Gimlin K, Ferriero DM, Noble-Haeusslein LJ. Brain development in rodents and humans: Identifying benchmarks of maturation and vulnerability to injury across species. Prog Neurobiol. 2013 DOI: 10.1016/j.pneurobio.2013.04.001
28. Chuang N, Mori S, Yamamoto A, Jiang H, Ye X, Xu X, et al. An MRI-based atlas and database of the developing mouse brain. Neuroimage. 2011 DOI: 10.1016/j.neuroimage.2010.07.043
29. Hammelrath L, Skokie S, Khmelinskii A, Hess A, van der Knaap N, Staring M, et al. Morphological maturation of the mouse brain: An in vivo MRI and histology investigation. Neuroimage. 2016 DOI:10.1016/j.neuroimage.2015.10.009
30. Chen Y, Kim H, Bok R, Sukumar S, Mu X, Sheldon RA, et al. Pyruvate to Lactate Metabolic Changes during Neurodevelopment Measured Dynamically Using Hyperpolarized 13C Imaging in Juvenile Murine Brain. Dev Neurosci. 2016 DOI: 10.1159/000439271
31. Dienel GA, Cruz NF. Imaging brain activation: Simple pictures of complex biology. Annals of the New York Academy of Sciences. 2008 DOI: 10.1196/annals.1427.011
32. Nedelcu J, Klein MA, Aguzzi A, Boesiger P, Martin E. Biphasic edema after hypoxic-ischemic brain injury in neonatal rats reflects early neuronal and late glial damage. Pediatr Res. 1999 DOI: 10.1203/00006450-199909000-00008
33. Hudome S, Palmer C, Roberts RL, Mauger D, Housman C, Towfighi J. The role of neutrophils in the production of hypoxic-ischemic brain injury in the neonatal rat. Pediatr Res. 1997 DOI: 10.1203/00006450-199705000-00002
34. Kraut JA, Madias NE. Lactic acidosis. N Engl J Med. 2014 DOI: 10.1056/NEJMra1309483
35. Paschen W, Djuricic B, Mies G, Schmidt-Kastner R, Linn F. Lactate and pH in the Brain: Association and Dissociation in Different Pathophysiological States. J Neurochem. 1987 DOI: 10.1111/j.1471-4159.1987.tb13140.x
36. Wu TW, Tamrazi B, Hsu KH, Ho E, Reitman AJ, Borzage M, et al. Cerebral lactate concentration in neonatal hypoxic-ischemic encephalopathy: In relation to time, characteristic of injury, and serum lactate concentration. Front Neurol. 2018 DOI: 10.3389/fneur.2018.00293
37. Vannucci RC, Yager JY. Glucose, lactic acid, and perinatal hypoxic-ischemic brain damage. Pediatr Neurol. 1992 DOI: 10.1016/0887-8994(92)90045-Z
38. Vannucci RC, Yager JY, Vannucci SJ. Cerebral glucose and energy utilization during the evolution of hypoxic-ischemic brain damage in the immature rat. J Cereb Blood Flow Metab. 1994 DOI: 10.1038/jcbfm.1994.35
39. Blomgren K, Hagberg H. Free radicals, mitochondria, and hypoxia-ischemia in the developing brain. Free Radic Biol Med. 2006 DOI: 10.1016/j.freeradbiomed.2005.08.040
40. Pellerin L, Pellegri G, Martin JL, Magistretti PJ. Expression of monocarboxylate transporter mRNAs in mouse brain: Support for a distinct role of lactate as an energy substrate for the neonatal vs. adult brain. Proc Natl Acad Sci U S A. 1998 DOI: 10.1073/pnas.95.7.3990

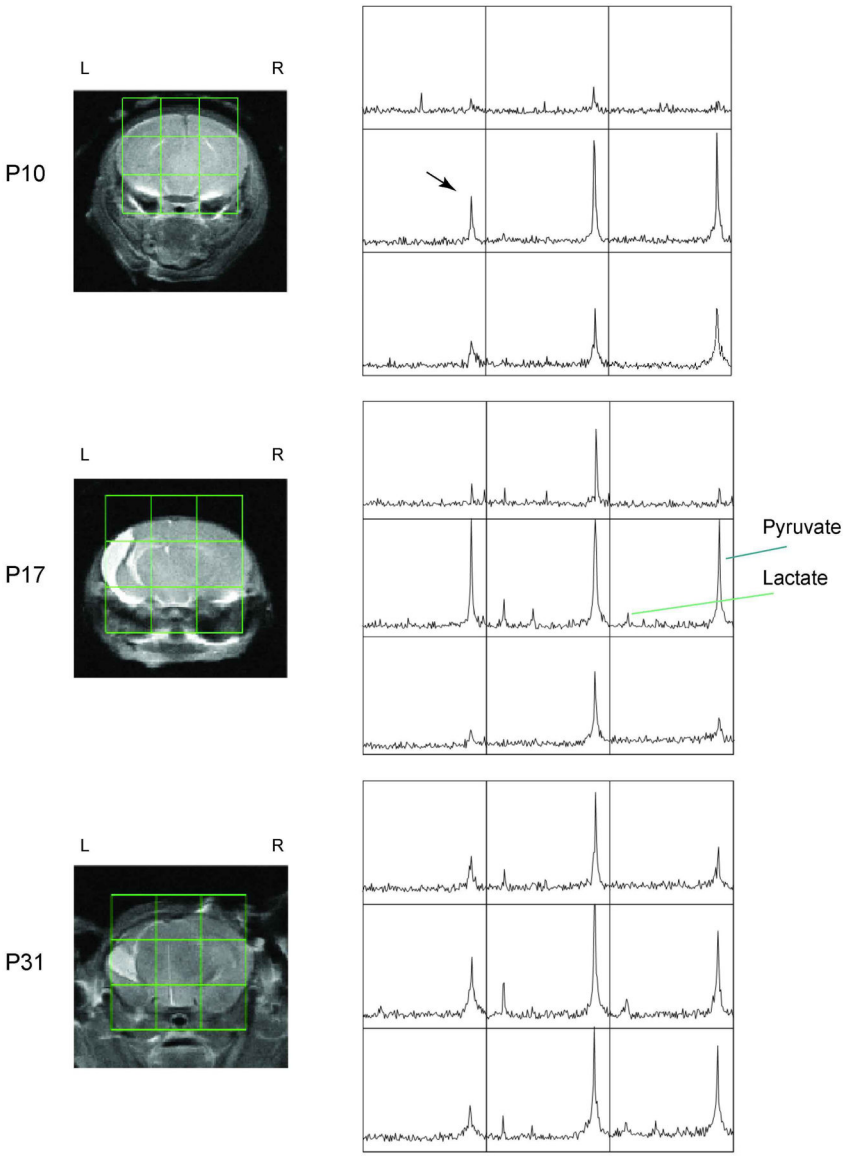

Figure 1.

T2-weighted images overlaid with ^{13}C spectroscopic imaging with matching orientation at P10, P17 and P31 of a representative subject. A slight hypointensity in the left hemisphere of the T2 weighted image and a significant reduction of pyruvate delivery in the spectra (arrow) can be observed a few hours after HI at P10. The reduction persists throughout P17 and P31 but is less pronounced.

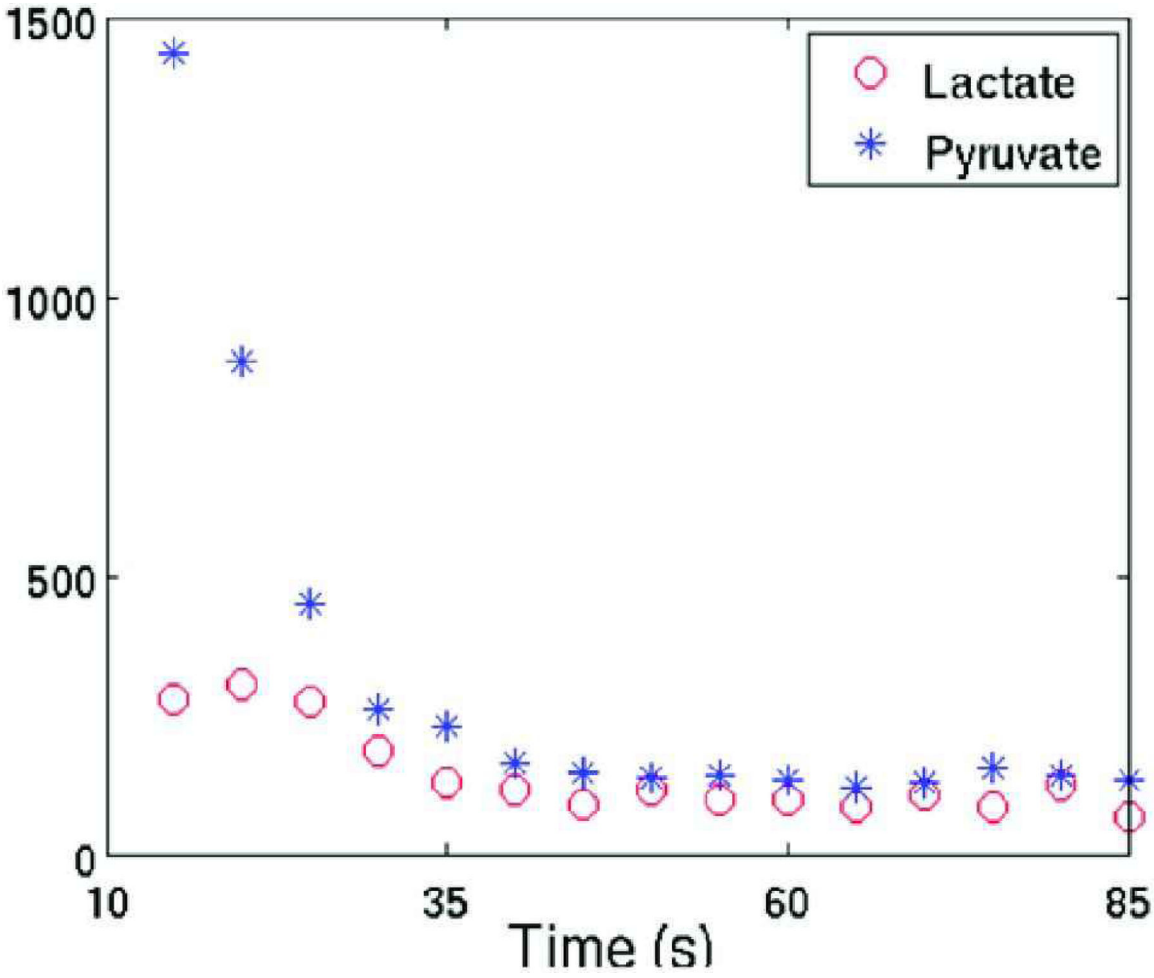

Figure 2.

Pyruvate and lactate signals from the start of acquisition (10th second) to the end of acquisition (85th second) with 5-second intervals. Pyruvate signal depicts decay over time. Lactate signal has a slight build-up due to its conversion from pyruvate, and then decay.

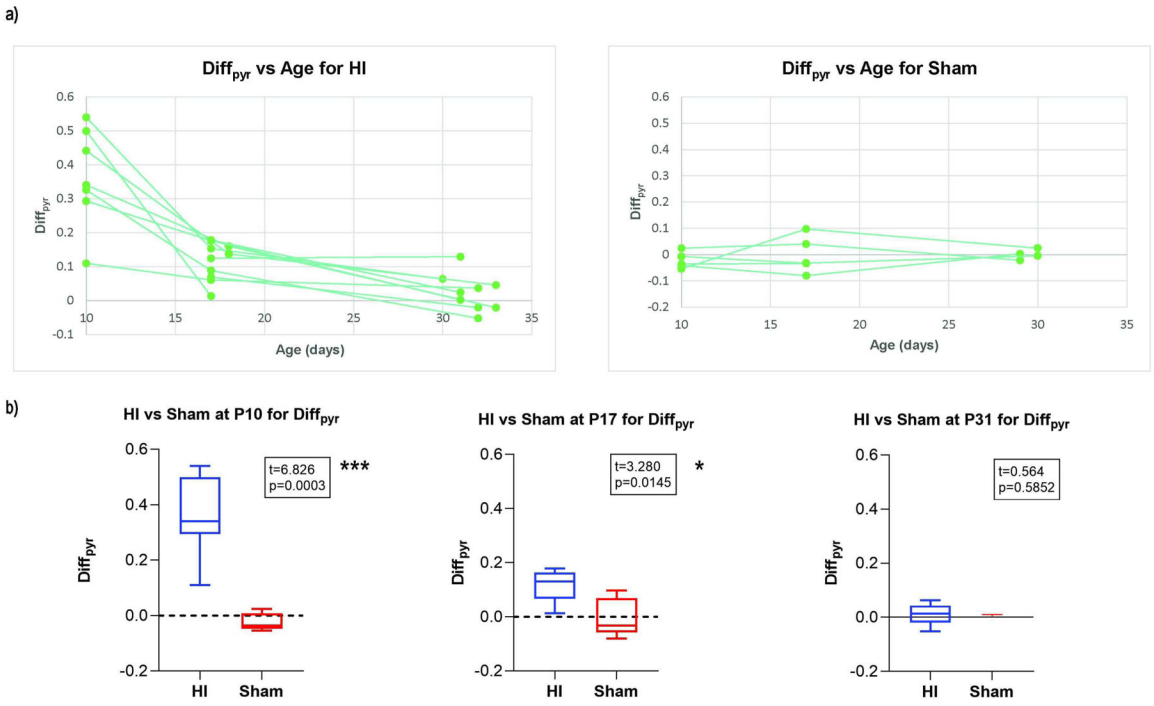

Figure 3.

(a) *Dif* f_{pyr} plotted again age for each subject in HI (n = 10) and sham (n = 5) groups. (b) Student's t-test for *Dif* f_{pyr} between HI and sham groups at each age time point. ***p<0.001, *p<0.05

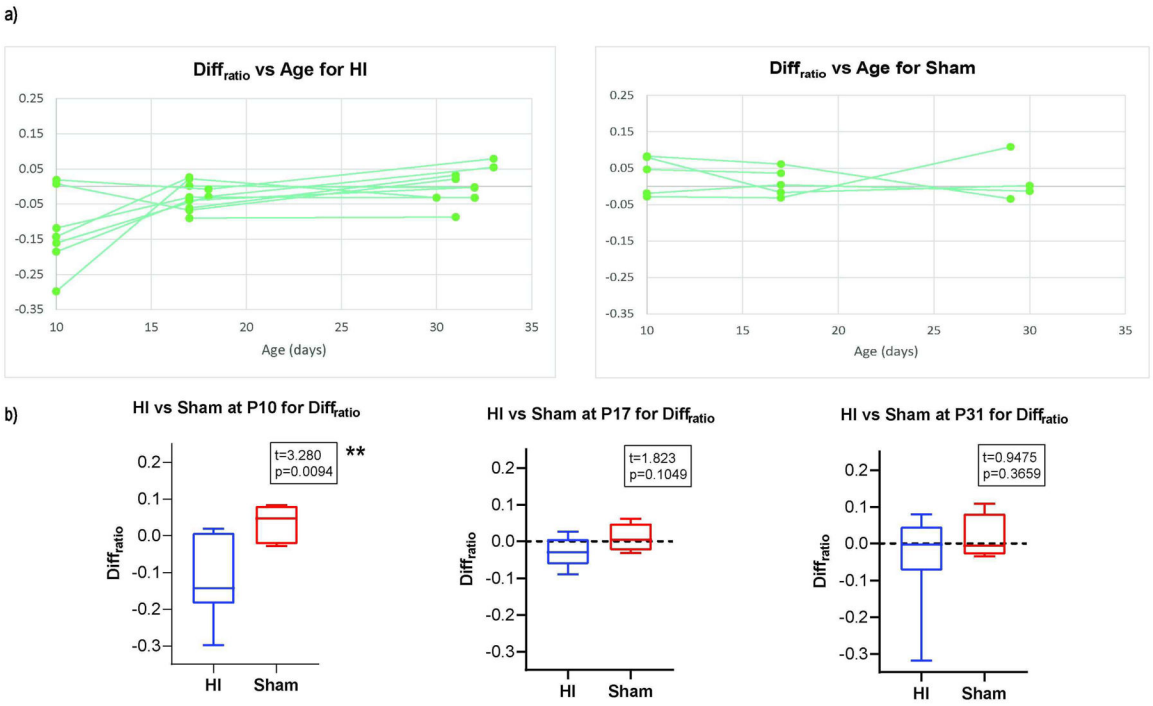

Figure 4.

(a) *Dif* f_{ratio} plotted again age for each subject in HI (n = 10) and sham (n = 5) groups. (b) Student's t-test for *Dif* f_{ratio} between HI and sham groups at each age time point. **p<0.01

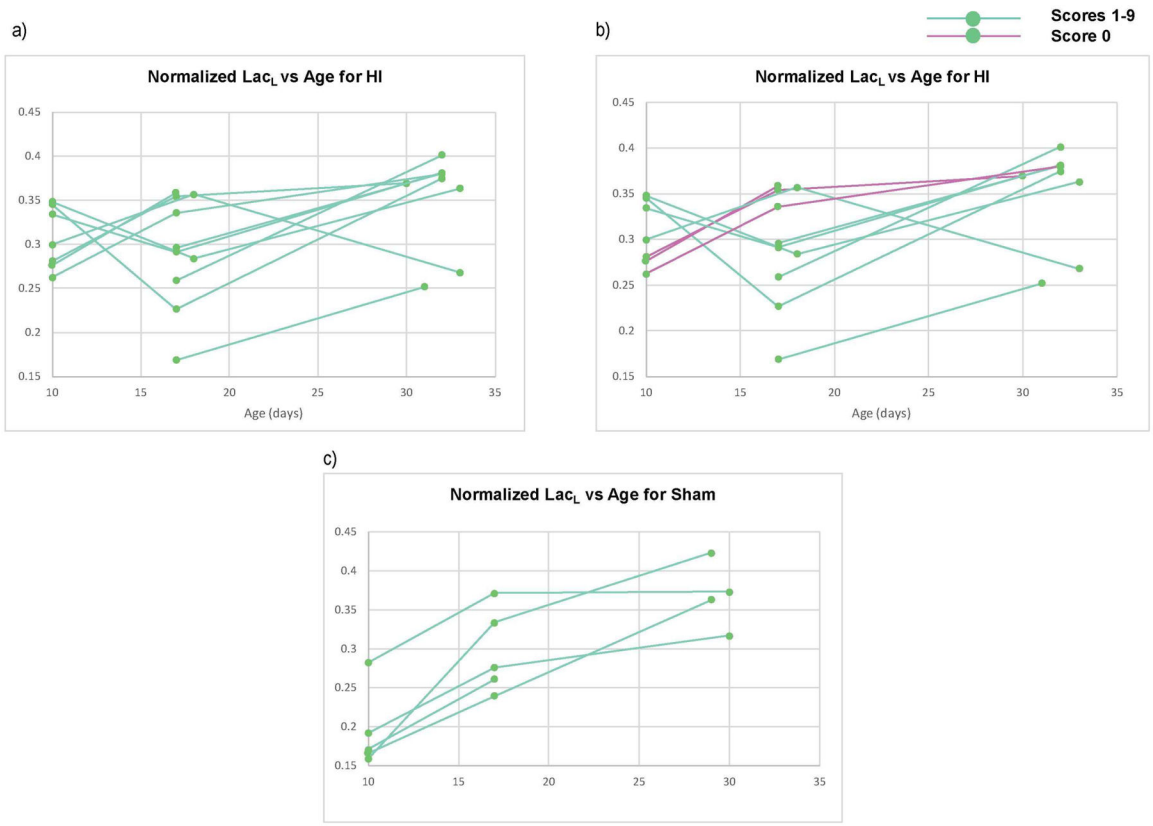

Figure 5.

(a) Normalized lactate levels in the injured hemisphere, plotted against age for each animal in (a) HI (n = 10), (b) HI with subgroups separated by injury scores (score=0 n=3; score=1–9: n=7), and (c) sham (n = 5) groups.

Table 1.

T2 injury scores for each animal in the HI group, at P17.

Mouse #	Cortex	Hippocampus	Deep Gray	Sum
1	3	3	0	6
2	0	0	0	0
3	0	2	0	2
4	3	3	1	7
5	3	2	2	7
6	3	2	2	7
7	3	3	3	9
8	0	1	0	1
9	0	0	0	0
10	0	0	0	0